



Aalborg Universitet

AALBORG UNIVERSITY
DENMARK

A new virtual-flux-vector based droop control strategy for parallel connected inverters in microgrids

Hu, Jiefeng; Zhu, Jianguo; Qu, Yanqing; Guerrero, Josep M.

Published in:
Proceedings of the 2013 IEEE ECCE Asia DownUnder

DOI (link to publication from Publisher):
[10.1109/ECCE-Asia.2013.6579157](https://doi.org/10.1109/ECCE-Asia.2013.6579157)

Publication date:
2013

Document Version
Early version, also known as pre-print

[Link to publication from Aalborg University](#)

Citation for published version (APA):
Hu, J., Zhu, J., Qu, Y., & Guerrero, J. M. (2013). A new virtual-flux-vector based droop control strategy for parallel connected inverters in microgrids. In *Proceedings of the 2013 IEEE ECCE Asia DownUnder* (pp. 585-590). IEEE Press. <https://doi.org/10.1109/ECCE-Asia.2013.6579157>

General rights

Copyright and moral rights for the publications made accessible in the public portal are retained by the authors and/or other copyright owners and it is a condition of accessing publications that users recognise and abide by the legal requirements associated with these rights.

- Users may download and print one copy of any publication from the public portal for the purpose of private study or research.
- You may not further distribute the material or use it for any profit-making activity or commercial gain
- You may freely distribute the URL identifying the publication in the public portal -

Take down policy

If you believe that this document breaches copyright please contact us at vbn@aub.aau.dk providing details, and we will remove access to the work immediately and investigate your claim.

A New Virtual-Flux-Based Droop Control Strategy for Parallel Connected Inverters in Microgrid

Jiefeng Hu, Jianguo Zhu, Yanqing Qu, and Josep M. Guerrero
University of Technology, Sydney, Australia Jiefeng.Hu@uts.edu.au
Aalborg University, Denmark joz@et.aau.dk

Abstract—Voltage and frequency droop method is commonly used in microgrids to achieve proper autonomous power sharing without rely on intercommunication systems. This paper proposes a new control strategy for parallel connected inverters in microgrid applications by drooping the flux instead of the inverter output voltage. Firstly, the relation between the inverter flux and the active and reactive power is mathematically obtained. Secondly, a novel flux droop method is then developed in order to regulate the active and reactive powers by drooping the flux amplitude and the phase angle, respectively. In addition, a small-signal model is developed in order to design the main control parameters and study the system dynamics and stability. The proposed control scheme includes a direct flux control (DFC) algorithm, which avoids the use of PI controllers and PWM modulators. Furthermore, in order to reduce the flux ripple, a model predictive control (MPC) scheme is integrated into the DFC. The obtained results shows that the proposed flux droop strategy can achieve active and reactive power sharing with much lower frequency deviation and better transient performance than the conventional droop method, thus which make it very attractive, highlighting the potential use in microgrid applications.

Index Terms—Microgrids, distributed generation, flux droop control, model predictive control, active and reactive power sharing

I. INTRODUCTION

THE rapid depletion, thus the increase of cost of fossil fuels, rising demand of electricity, and even tightening government policies on reduction of greenhouse gas emission, together with the inability and inefficiency of the existing electricity grid, are driving major changes in electricity generation and consumption patterns all around the world. In the last decade, serious concerns were raised about distributed generation units (DGs), such as wind turbines, photovoltaic (PV), gas microturbines, fuel cells and gas/steam powered combined heat and power (CHP) stations. More recently, microgrids have attracted much attention with the integration of DGs into the low voltage distribution network through inverters. Compared to a single DG, the microgrid has more capacity and control flexibilities to fulfill system reliability and power quality

requirements [1], [2].

The fast development of digital signal processors has brought about an increase in control techniques for the parallel operation of inverters in microgrid, among which the droop method is one of the most popular approaches [4]-[18]. This concept steams from the power system theory, in which a synchronous generator connected to the utility mains drops its frequency when the power demand increases. With this technique, the active and reactive power sharing by the inverters is automatic achieved by adjusting the output voltage frequency and amplitude. In order to fix the reference voltage generated by the droop controller, generally a multiloop control scheme is implemented, where an inner inductor current feedback loop and outer filter capacitor voltage feedback loop are used [5]-[18]. However, proportional-integral (PI) or proportional-resonant (PR) regulators are required, which complicate the control system. Besides, much turning effort is needed to obtain system stability, which makes it hard to be implemented. In [4], the voltage and frequency from the droop controller are delivered to the frequency controller and voltage control loops, respectively, to produce the referenced inverter flux. The inverter is then controlled to generate this specified flux using a direct flux method. However, this strategy is very complex and the system performance is compromised.

Recently much attention has been paid to improve the voltage droop method to obtain better transient performance and more accurated power sharing. For example, better transient response was obtained by introducing derivative-integral terms [9]-[12]. The power sharing accuracy was enhanced by employing a virtual power frame transformation or a virtual impedance [13]-[15]. In [16], an angle controller was proposed to minimize frequency variation by drooping the inverter output voltage angle instead of the frequency. However initial angle from the other inverters is not possible to know without using a GPS. The voltage deviation caused by droop method is compensated by a multilayer control strategy in [17] and [18]. However, all these methods are developed based on the voltage droop, i.e., $\omega - P$ and $V - Q$ characteristic, therefore, the conventional complex multi-feedback loops seems unavoidable. Besides, the proper power sharing is achieved at the expense of voltage deviation.

In this paper, the initial motivation is to try to develop an alternative droop method that can achieve active and reactive power sharing as well as the conventional voltage droop control,

and at the same time the control system can be simplified without using multi-feedback loops and PI controllers.

This paper is organized as follows. In Section II, the relation between the power flow and the inverter flux is deduced, based on which a new virtual-flux-vector-based droop control is proposed. In Section III, the small signal model is presented to help design control parameters and improve the system stability. In Section IV, a model predictive of direct flux control strategy is proposed to produce the virtual-flux reference of the droop controller. After that, the whole control strategy of the microgrid is described by combing the proposed flux droop method and the model-predictive direct flux control scheme in Section V. Finally, simulation results are provided to validate the effectiveness of the proposed strategy in Section VI.

II. PROPOSED VIRTUAL-FLUX-VECTOR DROOP CONTROL

In the conventional droop method, the control loop makes tight adjustment over the output voltage frequency and amplitude of the inverter, in order to compensate the active and reactive power unbalances. The question is: are there any other kinds of droop method to achieve load sharing rather than the conventional voltage droop control? In this Section, the mathematical relation between the inverter flux and the active and reactive powers delivered to the common ac bus will be obtained, based on a new droop method.

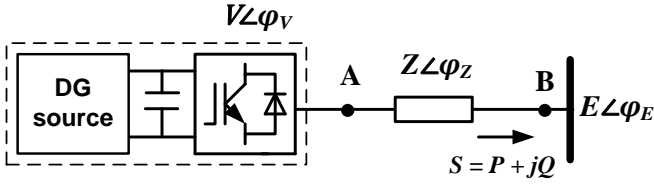


Fig. 1. Equivalent circuit of a DG unit connected to a common ac bus.

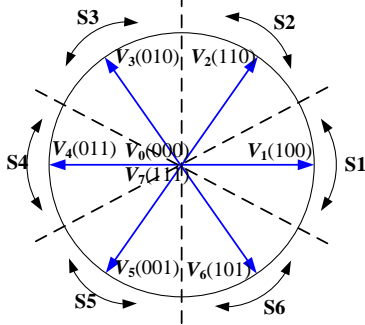


Fig. 2. Possible voltage vectors generated by the inverter.

A DG unit connected to a common ac bus through a power inverter is shown in Fig. 1. The three-phase two level inverter output voltage can be expressed in complex space vectors as follows

$$\mathbf{V}_i = \begin{cases} \frac{2}{3} V_{dc} e^{j(i-1)\frac{\pi}{3}} & (i = 1 \cdots 6) \\ 0 & (i = 0, 7) \end{cases} \quad (1)$$

being V_{dc} the voltage in the DC link and i the space voltage vector (from 0 to 7). Determined by the switching states, \mathbf{V}_i can be controlled to eight space voltage vectors, as shown in Fig. 2. The mathematical equation of the system equivalent circuit can be described as

$$\mathbf{V} = \mathbf{R}\mathbf{I} + L \frac{d\mathbf{I}}{dt} + \mathbf{E} \quad (2)$$

$$\mathbf{S} = \mathbf{P} + j\mathbf{Q} = \mathbf{I}^* \mathbf{E} \quad (3)$$

where \mathbf{V} , \mathbf{E} , and \mathbf{I} are the inverter output voltage vector, the common ac bus voltage vector, the line current vector, respectively; R is the line resistance, L is the line inductance, P and Q are the active and reactive powers that flow to the common ac bus. Super index $*$ denotes complex conjugate vector.

Similar to the flux definition in an electrical machine, the virtual flux vectors of at node A and at node B can be defined as

$$\boldsymbol{\psi}_V = \int_{-\infty}^t \mathbf{V} d\tau \quad (4)$$

$$\boldsymbol{\psi}_E = \int_{-\infty}^t \mathbf{E} d\tau \quad (5)$$

Consequently, the inverter flux vector $\boldsymbol{\psi}_V$ and the flux vector at node B $\boldsymbol{\psi}_E$ can be decomposed in phase and modules as following

$$\varphi_{fV} = \varphi_V - \frac{\pi}{2} \quad (6)$$

$$|\boldsymbol{\psi}_V| = \frac{|\mathbf{V}|}{\omega} \quad (7)$$

$$\varphi_{fE} = \varphi_E - \frac{\pi}{2} \quad (8)$$

$$|\boldsymbol{\psi}_E| = \frac{|\mathbf{E}|}{\omega} \quad (9)$$

where φ_{fV} and φ_{fE} are the phase angles of $\boldsymbol{\psi}_V$ and $\boldsymbol{\psi}_E$, respectively, while φ_V and φ_E are the phase angles of the voltage vector \mathbf{V} and the voltage vector \mathbf{E} , respectively; and ω is the angular frequency of the voltage vectors.

As in most practical cases, the line impedance is mainly inductive, so neglecting the line resistance and combining (2), (4) and (5) yields

$$\mathbf{I} = \frac{1}{L} (\boldsymbol{\psi}_V - \boldsymbol{\psi}_E) \quad (10)$$

By substituting (10) into (3), we can obtain

$$\mathbf{S} = \frac{1}{L} (\boldsymbol{\psi}_V - \boldsymbol{\psi}_E)^* \mathbf{E} \quad (11)$$

Again, substituting (6), (8) and (9) into (11) yields

$$\mathbf{S} = \frac{1}{L} (|\boldsymbol{\psi}_V| e^{j(\varphi_V - \frac{\pi}{2})} - |\boldsymbol{\psi}_E| e^{j(\varphi_E - \frac{\pi}{2})})^* \omega |\boldsymbol{\psi}_E| e^{j\varphi_E} \quad (12)$$

Consequently, the apparent power flows from the DG to the common ac bus can be derived as

$$\mathbf{S} = \frac{\omega}{L} \left[|\boldsymbol{\psi}_E| |\boldsymbol{\psi}_V| \sin(\varphi_V - \varphi_E) + j \left(|\boldsymbol{\psi}_E| |\boldsymbol{\psi}_V| \cos(\varphi_V - \varphi_E) - |\boldsymbol{\psi}_E|^2 \right) \right] \quad (13)$$

Therefore, the active power and reactive power can be expressed as

$$P = \frac{\omega}{L} |\boldsymbol{\psi}_E| |\boldsymbol{\psi}_V| \sin \delta \quad (14)$$

$$Q = \frac{\omega}{L} \left(|\boldsymbol{\psi}_E| |\boldsymbol{\psi}_V| \cos \delta - |\boldsymbol{\psi}_E|^2 \right) \quad (15)$$

where $\delta = \varphi_{fV} - \varphi_{fE}$, and normally δ is small enough that we can

assume $\sin(\delta) \approx \delta$ and $\cos(\delta) \approx 1$, and consequently obtain

$$P = \frac{\omega}{L} |\psi_E| |\psi_V| \delta \quad (16)$$

$$Q = \frac{\omega |\psi_E|}{L} (|\psi_V| - |\psi_E|) \quad (17)$$

Therefore, the active power flow is proportional to the flux phase angle difference δ and the reactive power flow is proportional to the flux magnitude difference ($|\psi_V| - |\psi_E|$). Based on the above analysis, we propose a new droop method by drooping the inverter output flux and the flux angle as

$$\delta = \delta^* - m(P^* - P) \quad (18)$$

$$|\psi_V| = |\psi_V|^* - n(Q^* - Q) \quad (19)$$

where δ^* is the nominal phase angle difference of ψ_V and ψ_E , $|\psi_V|^*$ is the nominal amplitude of the inverter flux; P^* and Q^* are the power rating of the DG unit; m and n are the slopes of the $P - \delta$ characteristics and the $Q - |\psi_V|$ characteristics, respectively. For illustration, consider the $P - \delta$ droop characteristics of a two-DGs microgrid, as shown in Fig. 3, the active power is dispatched between these two DGs by drooping their own flux angle difference δ . Once the load changes, the power outputs of both DG units will automatically change according to their $P - \delta$ droop characteristics to reach a new steady state.

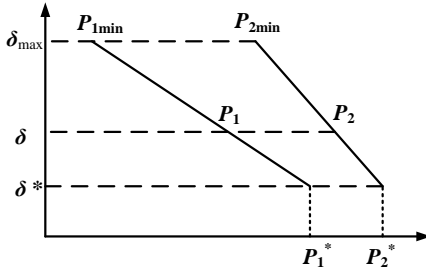


Fig. 3. $P - \delta$ characteristic.

III. DROOP CONTROLLER DESIGN AND STABILITY ANALYSIS

A. Small signal analysis

In order to analyze the system stability and the transient response, a small-signal analysis is provided, allowing the designer to adjust the main control parameters. The small-signal dynamics of the closed loop $P - \delta$ droop controlled system can be obtained by linearizing (14) and (18) as

$$\Delta\delta(s) = \Delta\delta^*(s) - m(\Delta P^*(s) - \Delta P(s)) \quad (20)$$

$$\Delta P(s) = G_p \cdot \Delta\delta(s) \quad (21)$$

where

$$G_p = \frac{\omega}{L} |\psi_E| |\psi_V| \cos \delta$$

Modeling the low-pass filters as a first-order approximation for the instantaneous active power calculation, the closed loop small signal model of the $P - \delta$ droop controller can be shown in Fig. 4.

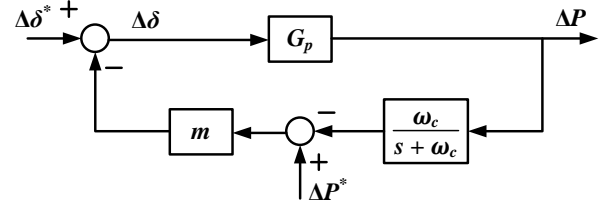


Fig. 4. Block diagram of the small signal model of the $P - \delta$ droop controller

By deriving the closed loop transfer function using ΔP as output and $\Delta\delta^*$ and ΔP^* as input according to the principle of superposition, one can obtain

$$\Delta P(s) = \frac{G_p(s + \omega_c)}{s + \omega_c - \omega_c m G_p} \Delta\delta^*(s) - \frac{m G_p(s + \omega_c)}{s + \omega_c - \omega_c m G_p} \Delta P^*(s) \quad (22)$$

where Δ denotes the perturbed values, and ω_c is the cut-off angular frequency of the low-pass filters.

The characteristic equation can be derived from (22) as

$$s + \omega_c - \omega_c m G_p = 0 \quad (23)$$

Subsequently, the eigenvalue of (23) can be expressed as

$$\lambda_p = \omega_c (m G_p - 1) \quad (24)$$

Similarly, the small-signal dynamics of the $Q - |\psi_V|$ droop controller can be obtained by linearizing (15) and (19) as

$$\Delta|\psi_V|(s) = \Delta|\psi_V|^*(s) - n(\Delta Q^*(s) - \Delta Q(s)) \quad (25)$$

$$\Delta Q(s) = G_q \cdot \Delta|\psi_V|(s) \quad (26)$$

where

$$G_q = \frac{\omega}{L} |\psi_E| \cos \delta$$

Using a similar procedure, one can obtain the $Q - |\psi_V|$ droop controller block diagram of the small signal model illustrated in Fig. 5.

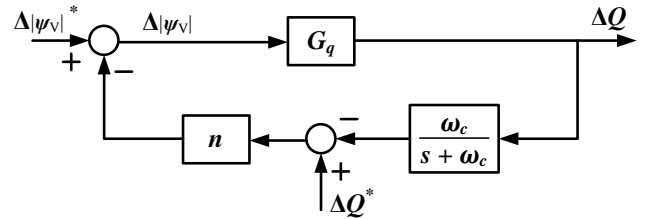


Fig. 5. Block diagram of the small signal model for the $Q - |\psi_V|$ droop controller.

By deriving the closed loop transfer function using ΔQ as output and $\Delta|\psi_V|^*$ and ΔQ^* as input according to the superposition principle, one can obtain

$$\Delta Q(s) = \frac{G_q(s + \omega_c)}{s + \omega_c - \omega_c n G_q} \Delta|\psi_V|^*(s) - \frac{n G_q(s + \omega_c)}{s + \omega_c - \omega_c n G_q} \Delta Q^*(s) \quad (27)$$

The characteristic equation can be derived from (27) as

$$s + \omega_c - \omega_c n G_q = 0 \quad (28)$$

Subsequently, the eigenvalue of (28) can be expressed as

$$\lambda_q = \omega_c (n G_q - 1) \quad (29)$$

According to (24) and (29), it can be seen that the eigenvalues placement of system varies with the droop slopes m and n , illustrating the stability limits which can be used to adjust the transient response of the system.

B. Coefficients Selection

The selection of the slopes m and n should take into account not only the system stability, but also the tradeoff between the power sharing accuracy and the flux deviation, which will influence the voltage and frequency deviation. Considering the system stability analysis based on the small signal model previously developed, here m and n are chosen to ensure steady state and system stability as

$$m = \frac{\delta^* - \delta_{\max}}{P^* - P_{\min}} \quad (30)$$

$$n = \frac{|\psi_V|^* - |\psi_V|_{\max}}{Q^* - Q_{\min}} \quad (31)$$

Since the power ratings of DGs and the nominal flux amplitude and phase angle difference are generally fixed for a given microgrid, consequently, the design of m and n is to adjust δ_{\max} , P_{\min} , $|\psi_V|_{\max}$, and Q_{\min} , taking into account the system stability, power sharing accuracy and the flux deviation.

IV. VIRTUAL-FLUX-VECTOR CONTROL

By using the conventional voltage droop method, the output of the droop controller generates the voltage reference, which is generally produced by using multi-loop approaches, i.e., outer voltage and inner current feedback control with PI regulators and a PWM modulator [5]-[18]. However, since the output of the proposed flux droop controller is the flux reference, thus direct flux control strategy can be employed to generate this specific flux reference as it has been shown to have good dynamic and steady state response [4].

In direct flux control, two variables that are controlled directly: $|\psi_V|$ and δ . In other words, the vector ψ_V is controlled to have a specified magnitude and a specified position relative to the vector ψ_E . For the switching-table-based direct flux control strategy (SDFC), the signals d_F and d_A are first obtained by two hysteresis comparators according to the tracking errors between the estimated and referenced values of $|\psi_V|$ and δ . The voltage vector is then selected from a look-up table (see Table I) according to d_F , d_A and the inverter flux position ϕ_{fV} . Being $d_F = 1$ if $|\psi_V|^* > |\psi_V|$ or $d_F = 0$ if $|\psi_V|^* < |\psi_V|$; and $d_A = 1$ if $\delta^* > \delta$, $d_A = 0$ if $\delta^* < \delta$. In the same Table, k is the sector number in the $\alpha - \beta$ plane given by ϕ_{fV} , as depicted in Fig. 2. In this way, ψ_V is controlled along an approximate circular path within specified hysteresis bands through the inverter switching. Inherited from direct control approaches, DFC features excellent dynamic performance without neither coordinate transformations nor modulators. The DFC scheme is illustrated in Fig. 6 of Section V.

TABLE I.

VECTOR SELECTION STRATEGY [4]

	Vector
$d_F = 1$	V_{k+1}
$d_F = 0$	V_{k+2}
Zero vector is applied to when $d_A = 1$	

In this section, we develop an overall control strategy for the parallel-operation of inverters in microgrid applications. Fig. 6 shows the block diagram of the control strategy of one inverter connected to the microgrid, including two control blocks, they are the proposed virtual-flux droop control and the proposed DFC strategy. In the virtual-flux droop control, the active and reactive powers P and Q supplied by the DGs to the load are calculated from the line current I and load-side voltage E , and then given to the flux droop function to obtain the reference flux. In the DFC strategy, the inverter flux is firstly estimated from the current inverter switching states [19], the reference flux from the droop controller is then generated using DFC algorithm.

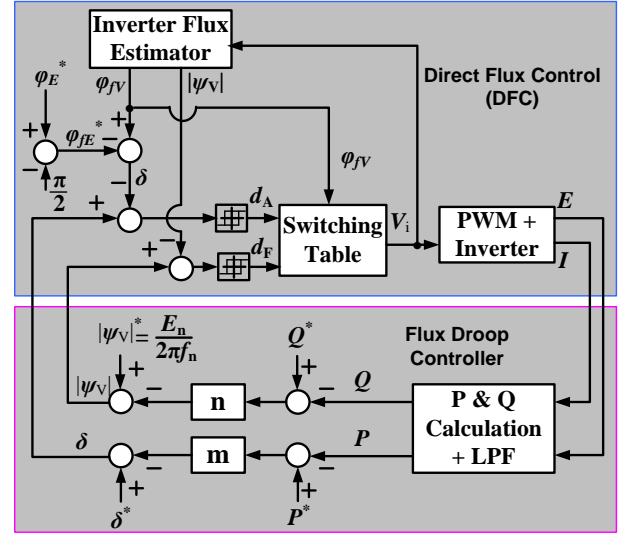


Fig. 6. Block diagram of the proposed microgrid control strategy

Notice that in islanded microgrids, there is no load-side ac voltage available for reference. The inverters themselves produce the ac system voltage. Actually by using the proposed control strategy of microgrids, the load-side ac voltage E is controlled indirectly because ψ_E is already regulated due to the direct control of ψ_V .

i) Amplitude Regulation: the amplitude of the load-side voltage E can be controlled by setting the nominal inverter flux amplitude $|\psi_V|^*$ equal to $2\pi f_n \cdot \sqrt{2}E_n / \sqrt{3}$, where E_n is the desired line-to-line voltage of the microgrid.

ii) Frequency Regulation: the referenced ϕ_{fE}^* is taken from a referenced virtual three-phase ac voltage E^* with $f_n = 60$ Hz, which can be calculated by $\phi_{fE}^* = \phi_E^* - \pi/2$, according to (8). In this way, ψ_E can be controlled with a specific frequency f_n because δ is tightly regulated, thus the frequency of the load-side voltage E can be controlled.

Now let us perform an in-depth analysis of the proposed flux droop method (18) in Section II. It can be seen that, in contrast to the conventional voltage droop method, the active power sharing of the microgrid is achieved by drooping the angle difference δ rather than drooping the frequency. Since the referenced ϕ_{fE}^* is taken from a virtual referenced three-phase ac voltage vector E^* with a constant frequency f_n , therefore, both the vector ψ_V and vector ψ_E will rotating with a constant angular

frequency because δ is tightly controlled. In other words, the angular frequency ψ_E will not be changed no matter how the δ is changed. Consequently, the active power sharing can be achieved without frequency deviation, even though the initial flux phase of each inverter is unknown. This is a significant improvement in microgrids since frequency regulation plays an important role.

VI. PERFORMANCE FURTHER ENHANCED USING MODEL PREDICTIVE CONTROL

The main drawback of the conventional SDFC is the large inverter flux ripples ($|\psi_V|$ and δ ripples). In the whole microgrid control (see Fig. 6), the steady-state and transient performance of the DFC strategy determines the performance of the power sharing of the microgrid system. Less flux ripples lead to less power ripples; better dynamic flux response results in better transient performance for the microgrid system to take up the load changes. This will be demonstrated in Section VII.

Here, enlighten from the model predictive control (MPC) of power electronics and electric drives [20]-[25], we propose a model predictive direct flux control (MPDFC) strategy to further reduce the inverter flux ripples and to improve the dynamic performance.

In fact, no matter if we use switching-table-based direct flux control of power converters or switching-table-based direct torque control of electric drives, the large inverter flux ripple (or torque ripple) is mainly due to the fact that the vector selected according to the switching table is not necessarily the best one in terms of reducing inverter flux ripple (or torque ripple), especially when the inverter flux (or rotor flux) position locates near the edge of sectors [26]. Therefore, it is expected that the voltage vectors are always chosen according to a specified criteria regardless of the inverter flux position.

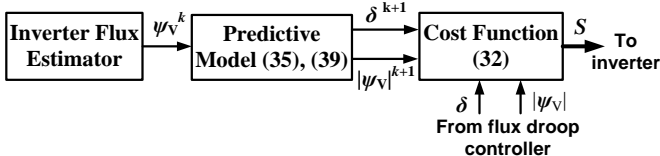


Fig. 8 Block diagram of proposed MPDFC strategy

The basic principle of the proposed MPDFC strategy is to use the system model to predict the system behavior at each sampling instant, the most appropriate voltage vector is then selected according to a cost function for the next sampling period, as illustrated in Fig. 7. Generally, different formulations of the cost function are possible, depending on which variables need to be controlled. In this paper, the cost function is chosen such that $|\psi_V|$ and δ can be as close to the referenced values as possible at the end of each sampling period, which can be defined as

$$J_{\min} = \sqrt{k_1(|\psi_V|^* - |\psi_V^{k+1}|)^2 + k_2(\delta^* - \delta^{k+1})^2} \quad (32)$$

where k_1 and k_2 are the weighting factors, $|\psi_V|^*$ and δ^* are the referenced inverter flux amplitude and the angle difference between ψ_V and ψ_E , respectively. In this application, weighting factors should be selected taking into account the trade-off

between the ripples reduction of $|\psi_V|$ and δ . After the cost function is defined, the next step is to predict the system behavior. According to (4), the inverter flux ψ_V^{k+1} can be predicted as

$$\psi_{Vd}^{k+1} = \psi_{Vd}^k + V_d T_s \quad (33)$$

$$\psi_{Vq}^{k+1} = \psi_{Vq}^k + V_q T_s \quad (34)$$

where T_s is the sampling period. Consequently, we can obtain

$$|\psi_V^{k+1}| = \sqrt{(\psi_{Vd}^{k+1})^2 + (\psi_{Vq}^{k+1})^2} \quad (35)$$

$$\phi_{fV}^{k+1} = \tan^{-1}\left(\frac{\psi_{Vd}^{k+1}}{\psi_{Vq}^{k+1}}\right) \quad (36)$$

On the other hand, in order to predict δ^{k+1} , ϕ_E^{k+1} should be obtained. For a three-phase ac voltage E , ϕ_E^{k+1} can be simply predicted as

$$\phi_E^{k+1} = \phi_E^k + \omega T_s \quad (37)$$

After obtain the phase angle of E , ϕ_{fE}^{k+1} can be calculated using (8) as

$$\phi_{fE}^{k+1} = \phi_E^{k+1} - \frac{\pi}{2} \quad (38)$$

Therefore, δ^{k+1} can be predicted as

$$\delta^{k+1} = \phi_{fV}^{k+1} - \phi_{fE}^{k+1} \quad (39)$$

After the system behaviors are also predicted, substitute (35) and (39) into (32), the voltage vector that produces minimum J will then be chosen to control $|\psi_V|$ and δ . The effectiveness of the MPDFC will be validated in Section VII.

VII. RESULTS AND DISCUSSIONS

Fig. 8 shows the test system of a two-DG based microgrid, which is identical as the one introduced in [4]. The system parameters are listed in Table II. The test was carried out using MATLAB/Simulink. The system sampling frequency is 20 kHz, the average switching frequency of each inverter is around 4.3 kHz. The load resistance R_{E2} is decreased suddenly to half its values at 0.16 s and the load reactance L_{L1} is decreased to half its values at 0.24 s for all the cases.

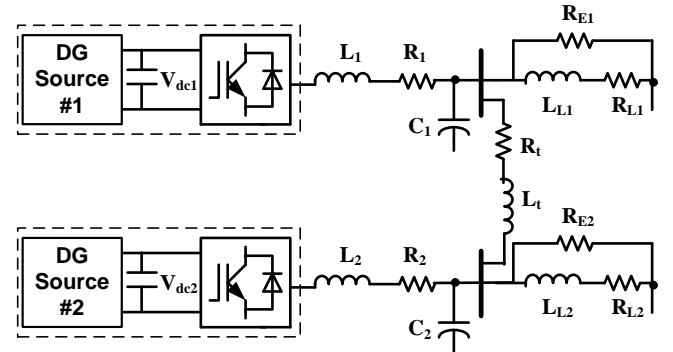


Fig. 8 Microgrid structure under study

TABLE II
SYSTEM PARAMETERS

Item	Symbol	Value	Unit
Line inductance	L_1, L_2	8	mH
Line resistance	R_1, R_2	0.05	Ω
Filter Capacitance	C_1, C_2	150	μF
Load inductance	L_{L1}, L_{L2}	40	mH
Load resistance	R_{L1}, R_{L2}	16	Ω
Load resistance	R_{E1}, R_{E2}	30	Ω
Tie-line inductance	L_t	6	mH
Tie-line resistance	R_t	0.4	Ω
Nominal line to line Voltage	E_n	3.6	kVrms
Nominal frequency	f_n	60	Hz
DGs output DC voltage	V_{dc1}, V_{dc2}	10	kV
Cut-off angular frequency	ω_c	10	rad/s
Nominal inverter flux amplitude	$ \psi_v ^*$	7.797	Wb
Nominal flux angle difference	δ^*	0.2	rads
Nominal active power of DG #1	P_1^*	0.75	MW
Nominal reactive power of DG	Q_1^*	0.2	MVAr
Nominal active power of DG #2	P_2^*	0.6	MW
Nominal reactive power of DG	Q_2^*	0.1	MVAr
Slope of $P - \delta$ droop of DG #1	m_1	-2.67×10^{-7}	rad/W
Slope of $Q - \psi_v $ droop of DG #1	n_1	-2.65×10^{-7}	Wb/VAr
Slope of $P - \delta$ droop of DG #2	m_2	-3.33×10^{-7}	rad/W
Slope of $Q - \psi_v $ droop of DG #2	n_2	-9.55×10^{-7}	Wb/VAr
Weighting factor 1	k_1	1	-
Weighting factor 2	k_2	16.2	-

A. Validation of the Proposed Flux Droop Control

Firstly, the effectiveness of the proposed flux droop control loop is tested, as illustrated in Fig. 6. The dynamic responses of the active and reactive powers sharing are shown in Fig. 9. It can be seen that the two DGs can take up the load changes immediately, the system reach a new steady-state within only 10 ms, and DG #1 carries a larger share of active power because it has a stiffer slope, as explained in Section II.

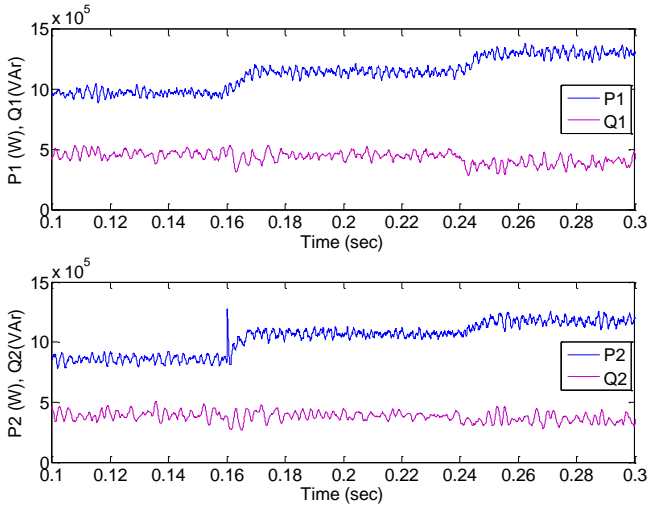


Fig. 9. Dynamic response of the active and reactive powers supplied by DGs to the loads.

Fig. 10 shows the inverters output currents supplied to the loads, while the load side voltages are shown in Fig. 11. It can

be seen that the local load benefits a very sinusoidal and stable voltage, before and after the load is changed.

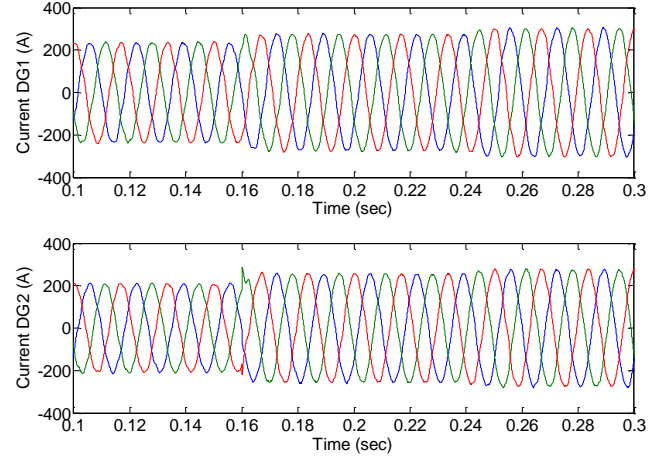


Fig. 10. Dynamic response of the currents supplied by DGs to the loads.

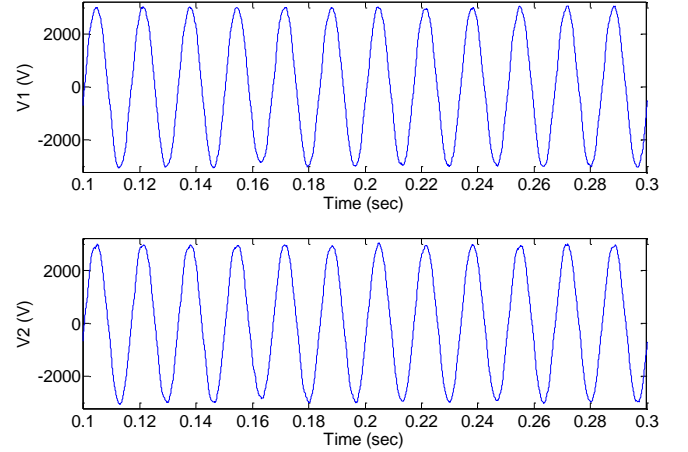


Fig. 11. Voltages response (a) voltage across C_1 of DG #1, (b) voltage across C_2 of DG #2.

B. Performance Enhanced by using MPC

In this test, one step was taken further to incorporate the model predictive direct flux control (MPDFC) with the proposed flux droop method. Fig. 12 shows the performance of the active and reactive powers supplied by DGs to the loads. Compared with Fig. 9, an overall improvement in steady-state and dynamic response of power sharing can be observed.

The performance improvement can be explained clearly in Fig. 13, which compares the internal behaviors of the proposed flux droop strategy around 0.16 s, using SDFC and MPDFC strategies, respectively. It can be found that δ (red curve) were decreased automatically in order to increase the active power output when the load changes according to the pre-defined $P - \delta$ characteristics, while no obvious change in $|\psi_v|$ (red curve) can be observed since there is no reactive power change in the load demand. Thanks to the excellent steady-state and dynamic performance of the MPDFC strategy, the actual values of $|\psi_v|$ and δ (blue curves) are better controlled to track the values (red curves) from the output of the flux droop controller, compared with the results using SDFC strategy.

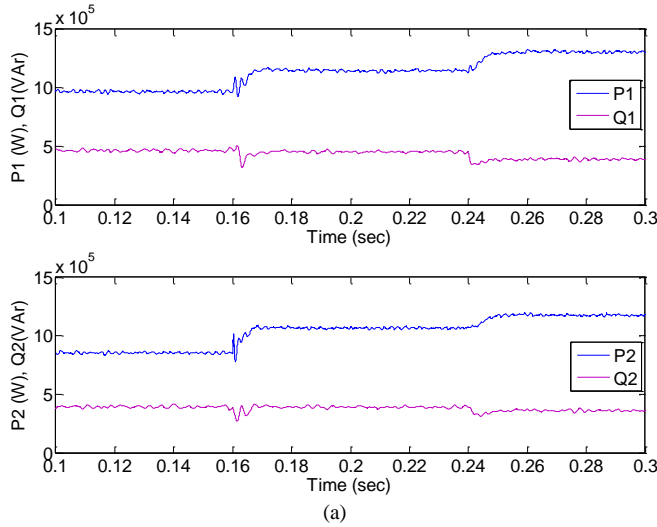


Fig. 12. Dynamic response of the active and reactive powers incorporating MPDFC with the flux droop control.

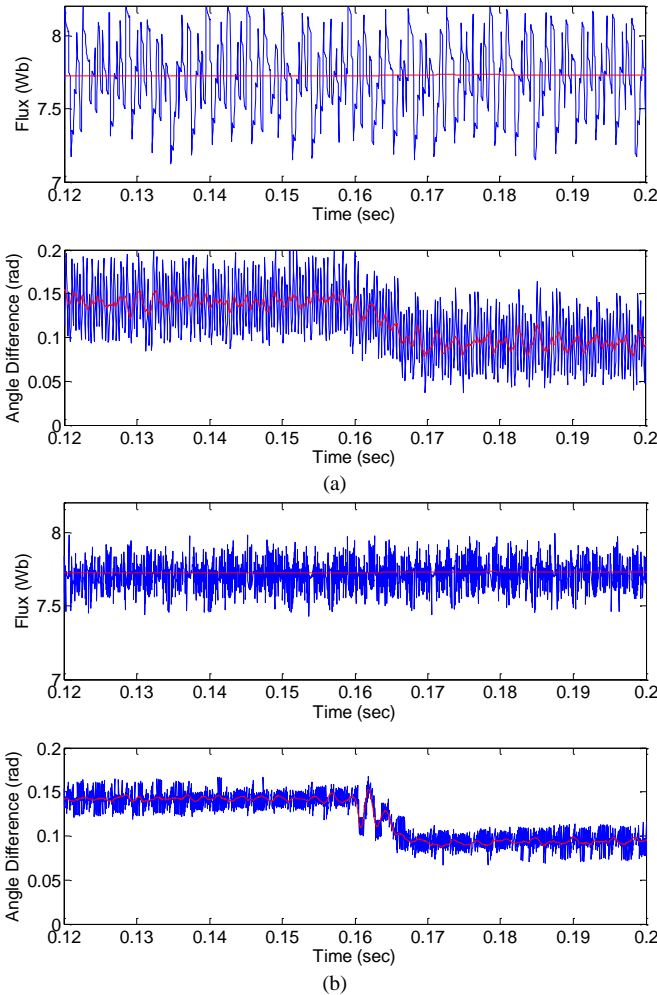


Fig. 13. Dynamic response of the flux droop controller of DG #1, (a) using SDFC, (b) using MPDFC.

C. Power Quality

Another main concern in microgrid control is the power quality, which is essential for the critical loads. Fig. 14 compares the line-to-line voltage across the filter capacitor C_1 of DG #1 at around 0.16 s. It can be found that the load side

voltage is more sinusoidal after using MPDFC, with 2.97% THD of SDFC and only 1.03% THD of MPDFC. The voltages performance presents a similar feature at around 0.24 s, so they are not shown here. Therefore, it is seen that MPDFC not only further improves the steady-state and dynamic performance of the power sharing, but also significantly improve the voltage quality.

In order to check the voltage deviation of the proposed flux control strategy, Table III compares the frequency deviation and amplitude deviations before and after load changes for the conventional voltage droop and the proposed flux droop. For the conventional droop control, the droop parameters are chosen as the one in [4]. It can be seen that there is about 7 V of voltage amplitude deviation in order to compensate 0.1 MVar reactive power unbalance, for both the $V-Q$ and $|\psi_V|-Q$ droop characteristics. However, if there is 0.1 MW of active power unbalance flowing, the frequency features 0.45 Hz deviation when using the conventional droop while only 0.02 Hz for the proposed flux droop.

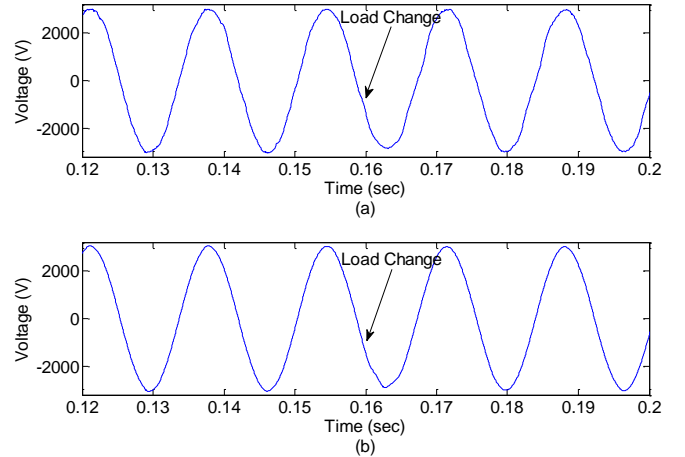


Fig. 13. Voltage across the capacitor C_1 of DG #1, (a) flux droop method + SDFC, THD=2.97%, (b) flux droop method + MPDFC, THD=1.03%.

TABLE III
VOLTAGE DEVIATIONS FOR $\Delta P = 0.1$ MW AND $\Delta Q = 0.1$ MVAR

Methods	Frequency Deviations (Hz)	Amplitude Deviations (V)
Voltage Droop	0.45	7.5
Flux Droop	0.02	6.9

VIII. CONCLUSION

In this paper, a flux droop control strategy for the parallel operation of inverters is proposed. Different to the conventional voltage droop method, the power sharing is achieved by drooping the flux amplitude and phase angle difference. In addition, a model predictive control based algorithm is developed to directly control the flux reference by the droop controller, thus the system transient performance is greatly improved. To summarize, there are several advantages of the proposed control strategy, which can be described as follows:

- 1) Improved steady-state and transient performance due to the direct control algorithm instead of the conventional voltage and current multi-loop feedback control, which would make the system more slow.
- 2) Less frequency deviation in order to achieve power sharing since the flux angle difference is drooped instead of

frequency. The voltage quality is further improved by incorporating a model predictive control scheme.

3) The control structure is simple and easy to implement, and no PI regulators and PWM modulators are required.

The high performance endowed by this controller points out its applicability in parallel inverters systems such as microgrids.

REFERENCES

- [1] J. M. Guerrero, F. Blaabjerg, T. Zhelev, K. Hemmes, E. Monmasson, S. Jemei, M. P. Comech, R. Granadino, and J. I. Frau, "Distributed generation: Toward a new energy paradigm" *IEEE Ind. Electron. Mag.*, Vol. 4, No. 1, pp. 52-64, 2010.
- [2] H. Farhangi, "The path of the smart grid," *IEEE Power and Energy. Mag.*, Vol. 8, No. 2, pp. 18-28, 2010.
- [3] X. Liu, P. Wang, and P. C. Loh, "A hybrid ac/dc microgrid and its coordination control," *IEEE Trans. Smart Grid*, vol. 2, no. 2, pp. 278-286, Jun. 2011.
- [4] M. C. Chandorkar, D. M. Divan, and R. Adapa, "Control of parallel connected inverters in standalone ac supply systems," *IEEE Trans. Ind. Appl.*, vol. 29, no. 1, pp. 136-143, Jan./Feb. 1993.
- [5] A. Tuladhar, H. Jun, T. Unger, and K. Mauch, "Parallel operation of single phase inverter modules with no control interconnections," in *Proc. IEEE APEC*, 1997, pp. 94-100.
- [6] U. Borup, F. Blaabjerg, and P. N. Enjeti, "Sharing of nonlinear load in parallel-connected three-phase converters," *IEEE Trans. Ind. Appl.*, vol. 37, no. 6, pp. 1817-1823, Nov./Dec. 2001.
- [7] L. Mihalache, "Parallel control technique with no intercommunication signals for resonant controller-based inverters," in *Conf. Rec. IEEE IAS Annu. Meeting*, 2003, pp. 1882-1889.
- [8] Y. Li, D. M. Vilathgamuwa, and P. C. Loh, "Design, analysis, and real-time testing of a controller for multibus microgrid system," *IEEE Trans. Power. Electron.*, vol. 19, no. 5, pp. 1195-1204, 2004.
- [9] J. M. Guerrero, L. G. Vicuna, J. Matas, M. Castilla, and J. Miret, "A wireless controller to enhance dynamic performance of parallel inverters in distributed generation systems," *IEEE Trans. Power. Electron.*, vol. 19, no. 5, pp. 1205-1213, 2004.
- [10] J. M. Guerrero, J. Matas, L. G. de Vicuna, M. Castilla, and J. Miret, "Wireless-control strategy for parallel operation of distributed-generation inverters," *IEEE Trans. Ind. Electron.*, vol. 53, no. 5, pp. 1461-1470, 2006.
- [11] A. M. Salamah, S. J. Finney, and B. W. Williams, "Autonomous controller for improved dynamic performance of AC grid, parallel-connected, single-phase inverters," *IET Gener. Trasm. Distrib.*, vol. 2, no. 2, pp. 209-218, 2008.
- [12] J. C. Vásquez, J. M. Guerrero, A. Luna, P. Rodríguez, and R. Teodorescu, "Adaptive droop control applied to voltage-source inverter operating in grid-connected and islanded modes" *IEEE Trans. Ind. Electron.*, vol. 56, no. 10, pp. 4088-4096, 2009.
- [13] K. D. Brabandere, B. Bolsens, J. V. Keybus, A. Woyte, J. Driesen, and R. Belmans, "A voltage and frequency droop control method for parallel inverters," *IEEE Trans. Power. Electron.*, vol. 22, no. 4, pp. 1107-1115, 2007.
- [14] J. M. Guerrero, L. Hang, and J. Uceda, "Control strategy for flexible microgrid based on parallel line-interactive UPS systems," *IEEE Trans. Ind. Electron.*, vol. 56, no. 3, pp. 726-736, March 2009.
- [15] Y. Li and C. N. Kao, "An accurate power control strategy for power-electronics-interfaced distributed generation units operating in a low-voltage multibus microgrid," *IEEE Trans. Power. Electron.*, vol. 24, no. 12, pp. 2977-2988, 2009.
- [16] R. Majumder, B. Chaudhuri, A. Ghosh, R. Majumder, G. Ledwich, and F. Zare, "Improvement of stability and load sharing in an autonomous microgrid using supplementary droop control loop," *IEEE Trans. Power System.*, vol. 25, no. 2, pp. 796-808, 2010.
- [17] M. Hua, H. Hu, Y. Xing, and J. M. Guerrero, "Multilayer control for inverters in parallel operation without intercommunications," *IEEE Trans. Power. Electron.*, vol. 27, no. 8, pp. 3651-3663, August 2012.
- [18] M. Savaghebi, A. Jalilian, J. C. Vasquez, and J. M. Guerrero, "Secondary control scheme for voltage unbalance compensation in an islanded droop-controlled microgrid," *IEEE Trans. Smart Grid.*, vol. 3, no. 2, pp. 797-807, 2012.
- [19] M. P. Kazmierkowski, R. Krishnan, and F. Blaabjerg, *Control in Power Electronics*. New York: Academic, 2002.
- [20] P. Cortés, M. P. Kazmierkowski, R. M. Kennel, D. E. Quevedo, and J. Rodríguez, "Predictive control in power electronics and drives," *IEEE Trans. Ind. Electron.*, vol. 55, no. 12, pp. 4312-4321, 2008.
- [21] R. Vargas, P. Cortes, U. Ammann, J. Rodríguez, and J. Pontt, "Predictive control of a three-phase neutral-point-clamped inverter," *IEEE Trans. Ind. Electron.*, vol. 54, no. 5, pp. 2697-2705, October 2007.
- [22] S. Kouro, P. Cortés, R. Vargas, U. Ammann, and J. Rodríguez, "Model predictive control – a simple and powerful method to control power converters," *IEEE Trans. Ind. Electron.*, vol. 56, no. 6, pp. 1826-1838, 2009.
- [23] S. Mariethoz and M. Morari, "Explicit model-predictive control of a PWM inverter with an LCL filter," *IEEE Trans. Ind. Electron.*, vol. 56, no. 2, pp. 389-399, February 2009.
- [24] M. Preindl, E. Schaltz, and P. Thogersen, "Switching frequency reduction using model predictive direct current control for high-power voltage sources inverters," *IEEE Trans. Ind. Electron.*, vol. 58, no. 7, pp. 2826-2835, 2011.
- [25] M. A. Perez, J. Rodríguez, E. J. Fuentes, and F. Kammerer, "Predictive control of AC – AC modular converters," *IEEE Trans. Ind. Electron.*, vol. 59, no. 7, pp. 2832-2839, July 2012.
- [26] G. S. Buja and M. P. Kazmierkowski, "Direct torque control of PWM inverter-fed AC motors – A Survey," *IEEE Trans. Ind. Electron.*, vol. 1, no. 4, pp. 744-757, 2004.